

# Determining the squark mass at the LHC

Vernon Barger <sup>1\*</sup>, Yu Gao <sup>2†</sup>, Andre Lessa <sup>3‡</sup>, Xerxes Tata <sup>4§</sup>

*1. Physics Dept. University of Wisconsin, Madison, WI 53706, USA*

*2. Dept. of Physics, University of Oregon, Eugene, OR 97403, USA*

*3. Dept. of Physics and Astronomy, University of Oklahoma, Norman, OK 73019 USA*

*4. Dept. of Physics and Astronomy, University of Hawaii, Honolulu, HI 96822, USA*

## Abstract

We propose a new way to determine the squark mass based on the shape of di-jet invariant mass distribution of supersymmetry (SUSY) di-jet events at the Large Hadron Collider (LHC). Our algorithm, which is based on event kinematics, requires that the branching ratio  $B(\tilde{q} \rightarrow q\tilde{Z}_1)$  is substantial for at least some types of squarks, and that  $m_{\tilde{Z}_1}^2/m_{\tilde{q}}^2 \ll 1$ . We select di-jet events with no isolated leptons, and impose cuts on the total jet transverse energy,  $E_T^{tot} = E_T(j_1) + E_T(j_2)$ , on  $\alpha = E_T(j_2)/m_{jj}$ , and on the azimuthal angle between the two jets to reduce SM backgrounds. The shape of the resulting di-jet mass distribution depends sensitively on the squark mass, especially if the integrated luminosity is sufficient to allow a hard enough cut on  $E_T^{tot}$  and yet leave a large enough signal to obtain the  $m_{jj}$  distribution. We simulate the signal and Standard Model (SM) backgrounds for  $100 \text{ fb}^{-1}$  integrated luminosity at 14 TeV requiring  $E_T^{tot} > 700 \text{ GeV}$ . We show that it should be possible to extract  $m_{\tilde{q}}$  to within about 3% at 95% CL — similar to the precision obtained using  $m_{T2}$  — from the di-jet mass distribution if  $m_{\tilde{q}} \sim 650 \text{ GeV}$ , or to within  $\sim 5\%$  if  $m_{\tilde{q}} \sim 1 \text{ TeV}$ .

PACS numbers: 14.80.Ly, 12.60.Jv, 11.30.Pb, 13.85.Rm

---

\*Email: barger@physics.wisc.edu

†Email: ygao3@uoregon.edu

‡Email: lessa@nhn.ou.edu

§Email: tata@phys.hawaii.edu

# 1 Introduction

Supersymmetry (SUSY) is one of the best-motivated extensions of the Standard Model (SM) [1]. There have been numerous studies of strategies by which superpartners may be discovered at the LHC. The SUSY reach of the LHC is usually expressed in terms of the masses of coloured gluinos and squarks, expected to be the most copiously produced sparticles [2, 3, 4]. More recently, the focus has shifted to how well sparticle properties can be determined at the LHC, with the most attention being paid to sparticle masses, the underlying motivation being that knowledge of the sparticle spectrum will lead us to the mechanism by which SM superpartners acquire their masses. The problem, of course, is that it is not possible to construct mass peaks because every SUSY event (in  $R$ -parity conserving SUSY models that we focus upon in this paper) includes two undetected neutralinos ( $\tilde{Z}_1$ ), which we take to be the lightest supersymmetric particle (LSP).

The variable  $M_{\text{eff}} \equiv \sum_{i=1}^4 E_T(j_i) + |E_T^{\text{miss}}|$  constructed from transverse energy ( $E_T$ ) provides a rough measure of the mass of the lighter of gluinos/squarks [5, 3]. The end point of the same flavour, opposite-sign dilepton mass spectrum, first mentioned in Ref.[6], yields a precise measurement of the *mass difference*,  $m_{\tilde{Z}_2} - m_{\tilde{Z}_1}$ , between neutralinos. Hinchliffe, Paige and collaborators [5] pioneered systematic studies of the information that may be gleaned from end-points of a variety of mass distributions in LHC event samples with cuts to select out SUSY events over SM backgrounds, and showed that (modulo some discrete ambiguities) in favourable cases with two-body decay cascades, it is sometimes possible to also construct the masses, rather than just mass differences: in this connection, see also Ref. [7]. Since then, other techniques have been suggested to obtain sparticle masses. These include the use of the  $m_{T2}$  variable [8], its cousins  $m_{T\text{Gen}}$  and related variables [9], as well as their generalization to asymmetric decays [10], the so-called matrix element method [11], the presence of kinematic cusps in distributions [12], or through multi-lepton channels [13].

In this paper, we propose a new way of measuring masses for the case of event topologies with one step cascade decays of the type:

$$P^{(1)} + P^{(2)} \rightarrow q^{(1)} + D^{(1)} + q^{(2)} + D^{(2)} \quad (1)$$

where  $P^{(i)}$  are the parent particles (squarks in our analysis) initially produced in the hard scattering,  $D^{(i)}$ s are the invisible (lightest SUSY particles, LSP) daughters of  $P^{(i)}$ , while each  $q^{(i)}$  manifests itself as a jet in the detector. None of the existing mass measurement methods allow for a separate determination of both the parent and daughter masses from just the process (1). For instance, the much-studied  $m_{T2}$  method yields a measure of  $(m_P^2 - m_D^2)/2m_P$  which, only if  $m_D^2/m_P^2 \ll 1$ , provides a measurement of the parent mass [14]. If more complicated decay chains [15] or several production processes [14] are accessible, it may be possible to extract the individual parent and daughter masses. The method presented here offers an alternative way of determining  $m_P$  (also in the regime  $m_D^2/m_P^2 \ll 1$ ) from the dijet invariant mass distribution, and relies on completely distinct kinematical features from the standard  $m_{T2}$  procedure.

In our analysis, we assume that the daughter LSP is a bino-like neutralino  $\tilde{Z}_1$ , while the parent is a right squark, which dominantly decay via  $\tilde{q}_R \rightarrow q\tilde{Z}_1$ .<sup>1</sup> Thus our signal from right

---

<sup>1</sup>If instead, the LSP is a wino-like neutralino,  $\tilde{q}_L$  would dominantly decay to charged or neutral winos. Since

squark pair production is exactly two hard jets, no isolated leptons or photons, together with missing transverse energy ( $E_T^{\text{miss}}$ ). It has been pointed out [16], and since confirmed [17, 18] that SM backgrounds to this signal can be controlled by requiring acollinear jets, even without the use of  $E_T^{\text{miss}}$ . If gluinos are marginally heavier than squarks, they decay to squarks and an undetectably soft jet, so that  $\tilde{g}\tilde{q}$  production then adds to the squark dijet signal. If gluinos are light enough so that squarks dominantly decay to gluinos, we do not have the dijet plus  $E_T^{\text{miss}}$  signal, and our analysis does not apply. Aside from our assumption about the mass ordering between gluinos and squarks and  $m_{\tilde{Z}_1} \ll m_{\tilde{q}}$ , we endeavor to leave our analysis as model-independent as possible, and at the same time realistic in that we include all complications due to contamination from other SUSY processes and SM background. We will see below that in addition to yielding  $m_{\tilde{q}}$  our analysis may also serve to approximately constrain  $m_{\tilde{g}}$ .

## 2 The acollinear dijet signal

The cross section for pair production of  $\tilde{q}_R$  is determined by SUSY QCD just in terms of  $m_{\tilde{g}}$  and  $m_{\tilde{q}_R}$ , independent of the details of any model. For the mass ordering of interest to us, the decay  $\tilde{q}_R \rightarrow q\tilde{g}$  is kinematically suppressed, so that right squarks dominantly decay to the (bino-like) LSP. SUSY contamination to the acollinear dijet signal is, of course, model-dependent. For definiteness, we assume gaugino mass unification at the GUT scale, take  $\mu = m_{\tilde{g}}$ ,  $\tan\beta = 10$ , and use the scalar mass unification condition  $m_{\tilde{q}}^2 \simeq m_{\tilde{\ell}}^2 + 0.7m_{\tilde{g}}^2$  as a guide to the slepton mass. These choices have little effect on the right squark signal other than restricting the gluino to be not much heavier than the squark, since otherwise the slepton becomes too light.

We use ISAJET v7.78 [19] for our simulation of the SUSY signal at the LHC. We assume a toy calorimeter with cell size  $\Delta\eta \times \Delta\phi = 0.05 \times 0.05$ , extending to  $|\eta| = 4$ . Here  $\eta, \phi$  denote the jet pseudo-rapidity and azimuthal angle. The hadronic calorimetry (HCAL) energy resolution is taken to be  $100\%/\sqrt{E_T} \oplus 5\%$ , where the two terms are combined in quadrature. The electromagnetic calorimetry (ECAL) energy resolution is assumed to be  $5\%/\sqrt{E_T} \oplus 0.55\%$ . We use the cone type ISAJET jet finding algorithm, with a cone size  $\Delta R \equiv \sqrt{\Delta\eta^2 + \Delta\phi^2} \leq 0.4$  to group HCAL energy depositions into jets. Jets are then defined to be hadronic clusters with  $E_T(\text{jet}) > 50$  GeV. Leptons with transverse momentum  $p_T(l) > 5$  GeV are defined to be isolated if the visible activity within a cone of  $\Delta R < 0.2$  about the lepton direction satisfies  $\Sigma E_T^{\text{cells}} < 5$  GeV.

In the analysis of our signal, we require exactly two jets with,

1.  $E_T(j) \geq 50$  GeV,
  2. azimuthal angle separation  $\Delta\phi_{jj} \leq 1.5$ ,
  3.  $E_T^{\text{tot}} \equiv E_T(j_1) + E_T(j_2) > 700$  GeV, and
  4.  $\alpha \equiv E_T(j_2)/m_{jj} \geq 0.5$ .
- (2)

where  $j_1, j_2$  are ordered by jet  $E_T$  ( $E_T(j_1) > E_T(j_2)$ ) and  $m_{jj}$  is the invariant mass of the two jets. We veto events with isolated leptons or a third jet with  $E_T(j) \geq 50$  GeV. These cuts and veto criteria have been shown to very effectively remove the QCD dijet background [17, 18].

---

the SM daughters of the chargino decays would be very soft, the analysis we describe for  $\tilde{q}_R$  would then apply to  $\tilde{q}_L$ .

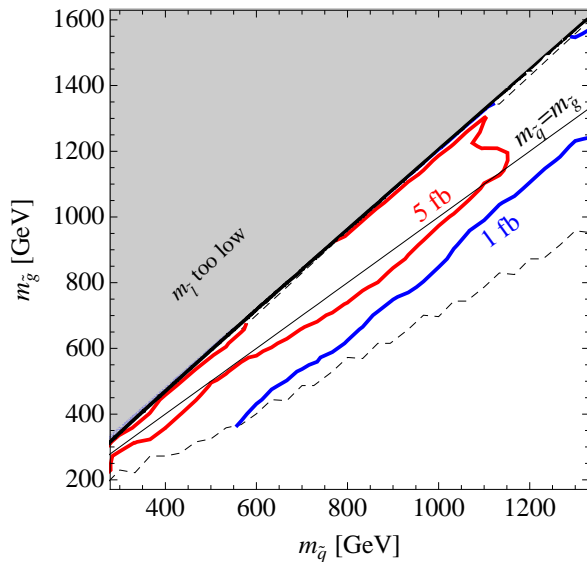


Figure 1: SUSY signal cross section contours for the acollinear dijet signal from supersymmetry at a 14 TeV  $pp$  collider, after cuts listed in Eq. (2). The dashed line shows the boundary of sampled area taken approximately to be  $m_{\tilde{g}} \simeq 0.7m_{\tilde{q}}$ . The upper left part of the plane is cut off because, for our choice of slepton masses, this region is forbidden either because the slepton is lighter than  $\tilde{Z}_1$  or  $m_{\tilde{l}}$  drops below 100 GeV. The cross section is largest just above  $m_{\tilde{q}} = m_{\tilde{g}}$  where it can easily exceed 10 fb.

The SM background is then dominated by  $(Z \rightarrow \nu\bar{\nu}) + jj$  events [17, 18], which has a cross section  $\sigma_{Zjj} = 6$  fb, with an additional contribution of  $\sigma_{Wjj} = 1.8$  fb from  $W \rightarrow \ell\nu$  events where the lepton is not identified.

Contours of the signal cross section at a 14 TeV  $pp$  collider after the cuts listed above are shown in the  $m_{\tilde{q}} - m_{\tilde{g}}$  plane in Fig. 1. We cut the contours off at large values of  $m_{\tilde{g}}$  where the slepton either becomes lighter than  $\tilde{Z}_1$ , or when it violates the LEP lower mass limit on its mass. The cross section drops off when  $m_{\tilde{g}}$  falls significantly below  $m_{\tilde{q}}$  because squark decays to gluinos begin to eat into the branching ratio  $B(\tilde{q} \rightarrow q\tilde{Z}_1)$ . The region where we terminate the 1 fb contour has recently been excluded at 95% CL by the CMS and ATLAS experiments at the LHC [20].

When the gluino is heavier than the squark the  $\tilde{g} \rightarrow \tilde{q} + \bar{q}$  decay channel opens up, and  $\tilde{g}\tilde{q}$  events can pass the  $N_j = 2$  cut if the  $\bar{q}$  forms a very soft jet, below the jet  $E_T$  threshold. This roughly doubles the signal just above the diagonal  $m_{\tilde{g}} = m_{\tilde{q}}$  line. However, this contribution falls off with increasing  $m_{\tilde{g}}$  (and fixed  $m_{\tilde{q}}$ ) because the additional jet becomes more readily identified in the detector. If instead  $m_{\tilde{g}} < m_{\tilde{q}}$ , the  $\tilde{q} \rightarrow \tilde{g} + q$  decay channel takes over quickly as the mass difference increases. This decay channel leads to multiple jets and the signal drops below 1 fb at  $m_{\tilde{g}} \sim \frac{4}{5}m_{\tilde{q}}$ . The signal is also suppressed at low  $(m_{\tilde{q}}, m_{\tilde{g}})$  due to the  $E_T^{tot}$  cut. Nevertheless, we see that there is a sizable region where there are several hundred events in the SUSY dijet channel for an integrated luminosity of  $100 \text{ fb}^{-1}$ .

### 3 Standard Model backgrounds

The dominant SM background to the SUSY signal in the acollinear dijet channel comes from the  $(Z \rightarrow \nu\bar{\nu}) + 2j$  events. Because the properties of jets in  $Z + 2j$  events at the LHC cannot depend on how the  $Z$  decays, this background can be directly obtained<sup>2</sup> by scaling LHC data on  $Z \rightarrow e^+e^- + \mu^+\mu^- + 2$  jet events by a factor,

$$\xi = \frac{BR(Z \rightarrow \nu\bar{\nu})}{BR(Z \rightarrow e^+e^-/\mu^+\mu^-)} \simeq 3.0. \quad (3)$$

The lower rate in the  $(Z \rightarrow \ell\bar{\ell}) + jj$  channel, however, implies that the fluctuations in the inferred background will be larger by  $\sqrt{\xi}$  relative to the corresponding fluctuations in the  $Z(\rightarrow \nu\bar{\nu}) + 2j$  sample. In our analysis we have used the Monte Carlo event generator AlpGen [21] to simulate the SM  $(Z \rightarrow \nu\bar{\nu}) + jj$  background, and then scaled the uncertainty in each  $m_{jj}$  bin by  $\sqrt{\xi}$  to correctly simulate the corresponding fluctuations when this background is obtained from the  $Z \rightarrow \ell\bar{\ell} + jj$  data.

In addition, as already mentioned,  $W + jj$  events make a subdominant but sizeable contribution to the background. Occasionally the charged lepton (most likely a hadronically decaying  $\tau$ ) from a high  $p_T$   $W$  decay becomes buried in the hadronic jets and/or is undetected because it is either too soft or in uninstrumented regions of the detector, while the neutrino is hard enough to reduce the angular separation of the two jets. The relatively small  $W + jj$  background compared to the leading  $Z + jj$  one reduces the relevance of  $W + jj$  contamination. While the subtraction of the  $Wjj$  background is not as simple as for the background from  $Zjj$  production, we may expect that the  $W + jj$  signal can be measured in a control region (such as the dijet + 1 lepton channel) and then extrapolated to the signal region (dijet + 0 leptons).<sup>3</sup> In our analysis, just as for the  $Zjj$  background, we assume that we can use AlpGen [21] to simulate and subsequently subtract the  $Wjj$  background from the total di-jet sample, but include the corresponding statistical uncertainty in the evaluation of  $\chi^2$  when performing our fits to extract sparticle masses.

The reader may well wonder whether it is further possible to enhance the SUSY signal relative to background via a requirement on  $E_T^{\text{miss}}$ . With this in mind, we show the  $E_T^{\text{miss}}$  distribution of SM  $Z/W + 2$  jet backgrounds in Fig. 2, along with the corresponding distribution for the two SUSY test cases that we introduce below for our study of how well the squark mass may be extracted at the LHC. The total SM background is 7.8 fb after the cuts in Eq. (2) to be compared with the signal of 16 fb (11 fb) for  $m_{\tilde{q}} = 650$  GeV (1 TeV). Note that the angular and  $E_T^{\text{tot}}$  cuts preclude very low values of  $E_T^{\text{miss}}$ . As the signal  $E_T^{\text{miss}}$  distribution moves to higher values with increasing  $m_{\tilde{q}}$ , it may appear tempting to impose an additional  $E_T^{\text{miss}}$  cut at 750 GeV to further enhance the signal events relative to the background. We have checked, however, that the loss in signal statistics largely negates the benefit of a lower background; the  $E_T^{\text{miss}}$  cut does not yield a significant improvement to the determination of  $m_{\tilde{q}}$ .

---

<sup>2</sup>Here, we are assuming that SUSY does not significantly contribute to  $Zjj$  events.

<sup>3</sup>This could be complicated by the fact that SUSY events may also make a contribution to the jets plus lepton channel, but typically, one would expect that the signal jet multiplicity is larger.

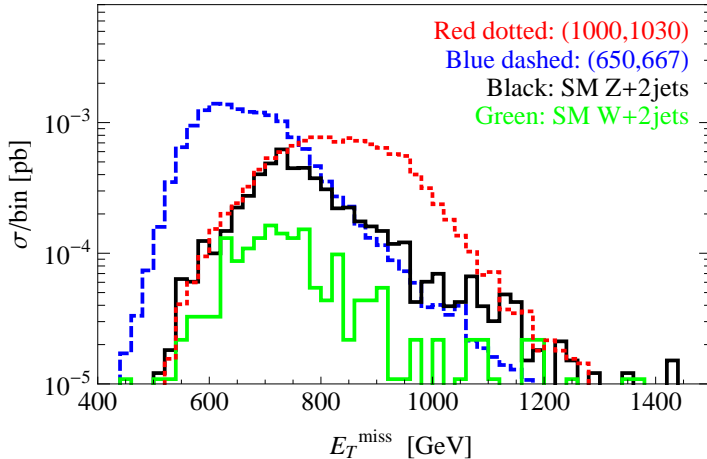


Figure 2: The  $E_T^{\text{miss}}$  distribution for the leading SM backgrounds from  $Z + jj$  and  $W + jj$  production, together with the same distributions for the signal points  $(m_{\tilde{q}}, m_{\tilde{g}}) = (650, 667)$  GeV and  $(1000, 1030)$  GeV at a 14 TeV  $pp$  collider after the cuts in Eq. (2). The  $Z + jj$  background shown here is the SM prediction for invisible  $Z$  decays and does not show the enhanced fluctuations that would result if this background were extracted from the  $(Z \rightarrow e^+e^-/\mu^+\mu^-) + jj$  data as discussed in the text.

## 4 Squark mass determination

### 4.1 Methodology

To facilitate the discussion of our strategy for squark mass determination, we show a scatter plot of the two jet energies in Fig. 3 for (a)  $m_{\tilde{q}} = 650$  GeV, and (b)  $m_{\tilde{q}} = 1$  TeV. Although we include *all* SUSY events in this sample, about 40% ( $> 90\%$ ) of the events come from squark pair production in frame (a) where the gluino-squark mass gap,  $\Delta M$ , is just 17 GeV, (in frame (b) with  $\Delta M = 30$  GeV) with the bulk of the remaining events arising from  $\tilde{g}\tilde{q}_R$  pair production. In the former case, although squark production seems to be subdominant, we should remember that the gluino decays into a squark and a (very soft) jet, so that these contaminating  $\tilde{g}\tilde{g}$  events have very similar kinematics as squark-pair events. Hence  $\tilde{g}\tilde{g}$  events do not interfere with our strategy to extract the squark mass and, in fact, help in that they increase the signal sample that we can use.<sup>4</sup>

The gray scale on the scatter plot shows how the events are distributed by invariant mass. We see that the bulk of events with low invariant dijet mass  $m_{jj}$  have small values of  $E_T(j_2)$  and (because of the  $E_T^{\text{tot}}$  cut) correspondingly large values of  $E_T(j_1)$ . This is not surprising since (except when both jets are very forward) our jet cone algorithm generally requires the jets to have a spatial angular separation between them, and precludes the smallest invariant masses if  $E_T(j_2)$  is also sizeable. Despite the fact that  $j_2$  is soft, these events readily satisfy

<sup>4</sup>If the gluino-squark mass gap becomes substantial, the additional jet from gluino decay frequently fails the third jet veto, suppressing the gluino signal. In case  $m_{\tilde{g}} \gg m_{\tilde{q}}$  the gluino production is suppressed and  $\tilde{q} \rightarrow q\tilde{Z}_1$  remains the only viable signal.

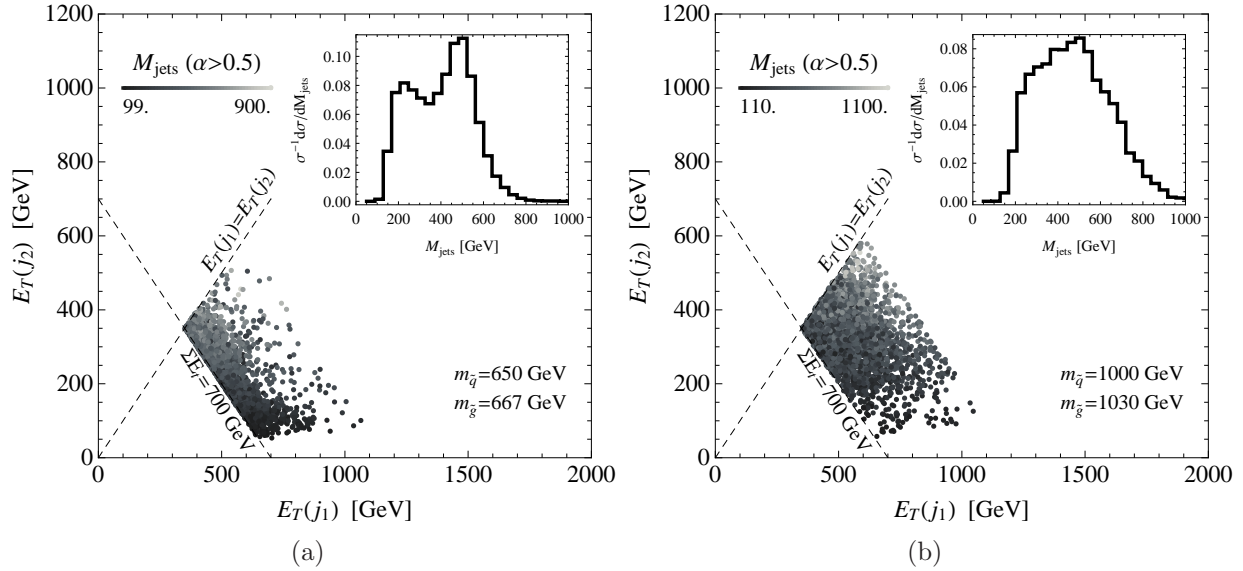


Figure 3: A scatter plot of the jet transverse energies for dijet events from supersymmetry at a 14 TeV  $pp$  collider for Frame (a)  $m_{\tilde{q}} = 650$  GeV, and Frame (b)  $m_{\tilde{q}} = 1$  TeV after the  $(\alpha, \Delta\phi_{jj}, E_T^{\text{tot}})$  cuts described in the text. The gluino mass is chosen slightly higher than the squark mass to enhance event rates by including gluino production channels. The invariant mass of the dijets is shown by the gray-scale on the dots. Notice that the region with the largest  $E_T(j_1)$  at the lower part of the plot is populated by events with low invariant mass, while events with high values of  $E_T(j_2)$  and of  $m_{jj}$  preferentially populate the upper part of the plot. This leads to the shoulders in the  $m_{jj}$  distribution for the 650 GeV squark case shown in the inset frame; this feature, absent for the 1 TeV squark case, would appear if we require  $E_T^{\text{tot}} > 1$  TeV.

the  $\alpha$  requirement because  $m_{jj}$  is also small. Relative to these events with the lowest values of  $m_{jj}$ , events with somewhat larger dijet masses are possible if *either*  $E_T(j_2)$  or the space angle between the jets is increased. If  $m_{jj}$  becomes larger because  $E_T(j_2)$  is increased, the  $\alpha$  cut is still satisfied. However, events with increased values of  $m_{jj}$  due to a larger angular separation but where  $E_T(j_2)$  remains small have smaller values of  $\alpha$ , and so a reduced efficiency for passing the  $\alpha > 0.5$  cut. We emphasize that *without the  $E_T^{tot}$  cut* these “intermediate  $m_{jj}$  events” would also be obtained for smaller values of  $E_T(j_1)$  and correspondingly larger values of  $E_T(j_2)$  that would readily satisfy  $\alpha > 0.5$ . Finally, events with large values of  $E_T(j_2)$  close to the  $E_T(j_1) = E_T(j_2)$  line naturally tend to have high values of dijet masses (as evidenced by the lack of dark points in this region of the scatter plot) as well as of  $\alpha$ . Of course, events with exactly back-to-back jets are *always* eliminated by the  $\alpha$  cut (and also the  $\Delta\phi$  cut), which is why this cut is an efficient veto against QCD dijet events.

To recap, these qualitative arguments suggest that, compared to events with very small or relatively large values of  $m_{jj}$ , events with intermediate values of dijet invariant mass are less likely to satisfy a hard cut on  $E_T^{tot}$  simultaneously with the requirement  $\alpha > 0.5$ . The dip in the di-jet invariant mass distribution near  $m_{jj} \sim 350$  GeV in Fig. 3(a) is a manifestation of exactly this feature. This deficit of intermediate events, as we will see below, which plays an important role in the extraction of  $m_{\tilde{q}}$  from the di-jet data, does not show up in the 1 TeV case in frame (b). To better understand this, we have analysed the kinematics of di-jet events from squark decay in the Appendix in more detail. In the approximation that the hard jet  $j_1$  is in the direction of its squark parent, we show that with  $E_T^{tot} > 2E_0 \equiv (m_{\tilde{q}}^2 - m_{\tilde{Z}_1}^2)/m_{\tilde{q}}$ , high mass events with large opening angle between the jets, as well as low mass events with a small opening angle between the jets readily satisfy that  $\alpha > 0.5$  requirement. We find, however, that intermediate mass events where the second jet is roughly perpendicular to the hard jet (in the squark CM frame) *can never* satisfy the  $\alpha$  cut if  $E_T^{tot} > 2.6E_0$ . Although our analysis in the Appendix neglects events from  $\tilde{g}\tilde{q}$  production for which the kinematics is slightly different because of the soft jet from gluino decay, and also any QCD radiation, it nevertheless confirms the general features that we inferred from our qualitative arguments of this Section. More importantly, it fixes the lower limit on  $E_T^{tot}$  in order for the dip to become apparent in the  $m_{jj}$  distribution to be  $\simeq 2E_0 \simeq m_{\tilde{q}}$  if  $m_{\tilde{Z}_1} \ll m_{\tilde{q}}$ . We now understand why we do not see a corresponding dip in Fig. 3 (b) — the  $E_T^{tot} > 700$  GeV cut is not hard enough, and the would-be dip region is populated by events with not-so-large values of  $E_T(j_1)$ , and concomitantly larger values of  $E_T(j_2)$  that then pass the  $\alpha > 0.5$  cut. Indeed, we have verified that by hardening the  $E_T^{tot}$  cut to 1 TeV we recover the dip also in this case. We have not shown this because the event rate then becomes too small; *i.e.* despite the appearance of the dip the reduced event rate does not lead to any improvement in the determination of  $m_{\tilde{q}}$ , at least for an integrated luminosity of  $100 \text{ fb}^{-1}$ . For this reason, we leave the  $E_T^{tot}$  cut at 700 GeV throughout this analysis.

We fit the synthetic  $m_{jj}$  data for the cuts in (2) to theoretical templates for a grid of  $(m_{\tilde{q}}, m_{\tilde{g}})$  in order to extract the squark mass. We use an integrated luminosity of at least  $1000 \text{ fb}^{-1}$  to generate these templates. We will see below that the squark mass can be extracted with greater precision if the integrated luminosity is sufficient for the implementation of a large enough  $E_T^{tot}$  cut so that the dip structure in the di-jet mass distribution (which is very sensitive to  $m_{\tilde{q}}$ ) is clearly evident.



## 4.2 Results

We now discuss the precision with which the squark mass can be extracted via fits to the di-jet mass distribution. We use the  $m_{\tilde{q}} = 650$  GeV and  $m_{\tilde{q}} = 1000$  GeV cases introduced above as illustrative examples. In order to extract the squark mass we fit the *shape* of the signal  $m_{jj}$  distribution — obtained after statistical subtraction of the backgrounds from the signal plus background sample as explained in Sec. 3 — to the corresponding distributions obtained using templates that have been independently generated for a grid of values of  $(m_{\tilde{q}}, m_{\tilde{g}})$ . Given that a signal has been detected in the di-jet sample, we define  $\chi^2$  for the normalized signal spectrum  $\phi^0 \equiv \frac{1}{N_0} \frac{dN_0}{dm_{jj}}$  as,

$$\chi^2(\phi) = \sum_i \frac{(\phi_i - \phi_i^0)^2}{\delta_{i,\phi^0}^2 + \delta_{i,Zjj}^2 + \delta_{i,Wjj}^2}, \quad (4)$$

where  $i$  sums over all  $m_{jj}$  bins, each one 30 GeV wide, and bins with less than 5 signal events are dropped. Here,  $\phi_i^0$  correspond to the “data” for  $100 \text{ fb}^{-1}$  in the  $i$ th bin, while  $\phi_i$  is the corresponding expectation for the value of  $(m_{\tilde{q}}, m_{\tilde{g}})$  from the template obtained with an integrated luminosity exceeding  $1000 \text{ fb}^{-1}$ . The uncertainty  $\delta_i \equiv \sqrt{N_i^{stat}/N_0^{tot}}$  gives the statistical error in the shape of signal spectrum after background subtraction. In this analysis we do not include systematics. We minimize  $\chi^2(\phi)$  over a grid in  $(m_{\tilde{q}}, m_{\tilde{g}})$  values, with its minimum being the best fit for  $(m_{\tilde{q}}, m_{\tilde{g}})$ , and as usual map out contours of constant  $\Delta\chi^2$  in the  $m_{\tilde{q}}-m_{\tilde{g}}$  plane. As mentioned in Sec. 2, gluino events only contribute to the signal if  $m_{\tilde{g}} \sim m_{\tilde{q}}$ . The gluino contribution improves the signal statistics but also has a small effect in the  $m_{jj}$  shape, and so affects the sparticle mass extraction as will be discussed shortly.

We note that Eq. (4) assumes perfect evaluation of the theoretical spectrum  $\phi_i$ . In practice, although we use an order of magnitude larger integrated luminosity for the calculation of the expectation from the templates, significant fluctuations remain distorting and even fragmenting the  $1\sigma$  (68% confidence level (CL)) contour. For this reason, we only show results for the extraction of sparticle masses at the  $2\sigma$  and  $3\sigma$  contours in the following.

Fig. 4 illustrates the results of our fit of the di-jet mass spectrum after the cuts of Eq. (2) for the two SUSY cases. The inner (outer) line corresponds to the  $2\sigma$  ( $3\sigma$ ) contour where  $\Delta\chi^2 = 6.2$  (11.8) above the minimum value of  $\chi^2$ . The reader may be surprised to see that the di-jet distribution also serves to constrain the gluino mass. To understand this, we note that starting from the best fit value, as we reduce  $m_{\tilde{g}}$  (keeping  $m_{\tilde{q}}$  fixed), squark decays to gluino open up and start to eat into the branching ratio  $B(\tilde{q} \rightarrow q\tilde{Z}_1)$ . When the gluino is only just a very tiny bit below  $m_{\tilde{q}}$ , it decays via  $\tilde{g} \rightarrow q\tilde{q}^*$ , with the virtual squark almost on its mass shell, and the additional quark jet being too soft for detection. The virtual almost-on-shell-squark then decays via  $\tilde{q}^* \rightarrow q\tilde{Z}_1$  and the fit is almost unaffected because events from squark decays to gluinos cannot be kinematically distinguished from events with squarks decaying to the LSP. However, as the gluino-squark mass difference increases, (1) gluino decays of squarks become more significant and begin eating into the branching fraction for LSP decays, and (2) the quark daughter of the squark becomes harder and so more likely to be detected. Indeed, if all  $\tilde{q} \rightarrow \tilde{g}q$  decays would be vetoed by our jet-multiplicity cut, all that would happen would be a loss of statistics, causing the ellipse to widen, and ultimately open up, for lower values of  $m_{\tilde{g}}$ . However, before this can happen, the three-body gluino decay still has quasi-two-body kinematics, but

with an off-shell squark lighter than  $m_{\tilde{q}}$ . As a result the template gluino events will be similar to squark events with a smaller squark mass; this alters the shape of the corresponding  $m_{jj}$  distribution, enabling the ellipse to close at low gluino masses.

If on the other hand, starting from the best fit value we now go up in  $m_{\tilde{g}}$  (again keeping  $m_{\tilde{q}}$  fixed), the gluino decays via  $\tilde{g} \rightarrow q\tilde{q}$ . Initially, the quark from the gluino is very soft, and gluinos simply act as a source of on-shell squarks. Thus  $\tilde{q}\tilde{g}$  production just leads to better statistics, and so lead to a more precise determination of  $m_{\tilde{q}}$ , as we have already noted. As the template value of  $m_{\tilde{g}}$  is increased with  $m_{\tilde{q}}$  fixed, the  $E_T$  distribution of the daughter squark from gluino decay, and hence of its daughter jet, is affected. Moreover, the quark daughter of the gluino becomes increasingly more likely to be detected, and events with gluinos are more likely to be vetoed. These effects combine and together lead to an increase of  $\Delta\chi^2$ . Note, however, that the quark daughter of the gluino will not be significantly harder if the template squark mass is also increased along with the template gluino mass, so that the template mass gap is still small. In this case, the effect that we have just mentioned is somewhat ameliorated, causing the error ellipses to tilt to the right as well as narrow in the squark direction as they extend to larger gluino (and squark) masses.<sup>5</sup>

We see from Fig. 4 that this analysis constrains the squark mass at  $2\sigma$  to:

$$\begin{aligned} (m_{\tilde{q}}, m_{\tilde{g}}) = (650, 667) \text{ GeV} & : m_{\tilde{q}} = 635 - 690 \text{ GeV} \\ (m_{\tilde{q}}, m_{\tilde{g}}) = (1, 1.03) \text{ TeV} & : m_{\tilde{q}} = 935 - 1040 \text{ GeV} \end{aligned} \quad (5)$$

The better precision in the first case is partly due to the fact that the higher statistics allows us to make use of the dip structure that we discussed in Sec. 4.1. We note also that the gluino mass is constrained to lie between 630-760 GeV (940-1220 GeV) in the two cases, with the true value being significantly closer to the lower end of the range.

## 5 A comparison with squark mass determination using

### $m_{T2}$

In this section we briefly examine how the extraction of the squark mass from the di-jet mass distribution compares with the corresponding determination using the  $m_{T2}$  variable [8] that has received extensive attention during the last few years. There is no question that, as we have already mentioned in Sec. 1 an  $m_{T2}$  analysis can potentially lead to a simultaneous determination of gluino and LSP masses [14] if squarks are heavy. Here, we focus our attention on the more difficult case that the squark is essentially degenerate with the gluino, in which case the kink structure on which the gluino and LSP mass determination is based is less evident [14]. For comparison purposes, we focus on acollinear di-jet events with the set of cuts Eq. (2) for the same test cases in Fig. 4. As in Sec. 4.2, we assume that the SM backgrounds ( $Z + jj$  and  $W + jj$ ) can be subtracted, but still include these in our analysis of the statistical significance of the signal.

---

<sup>5</sup>If however,  $m_{\tilde{g}} \gg m_{\tilde{q}}$  the rate of gluino events would be less frequent, and squark events for this case would differ from those for the test point only by changes in the squark  $E_T$  distribution and the event rate due to the much larger value of  $m_{\tilde{g}}$ . It is conceivable, therefore, that there is another region (well into the grey region in the figure) where  $\Delta\chi^2$  is reduced. We have not investigated whether this does indeed occur.

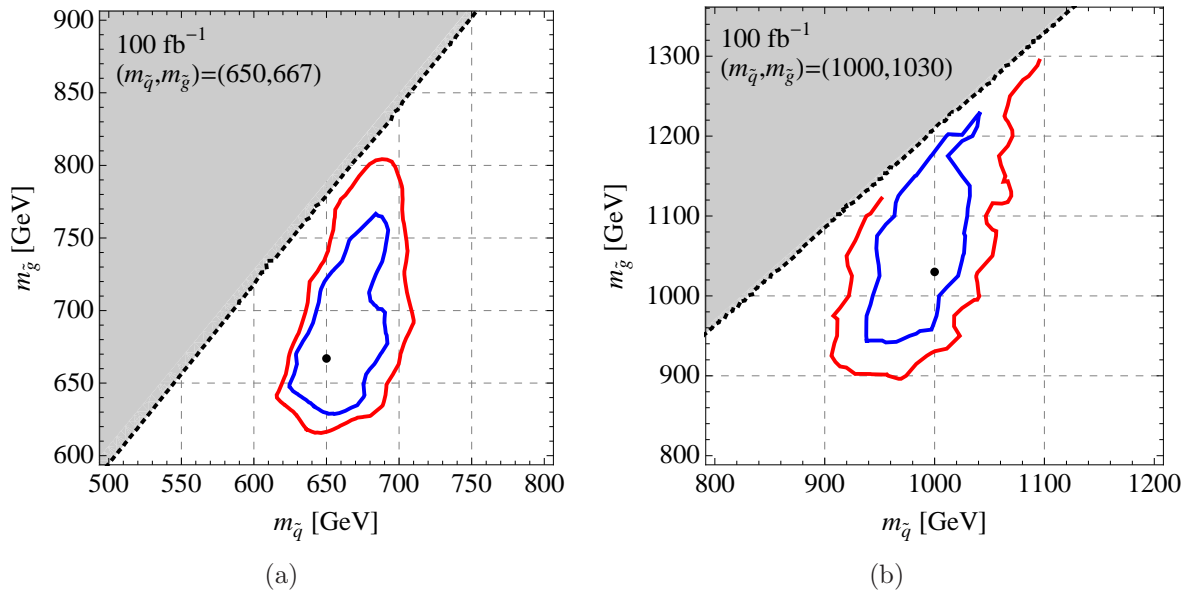


Figure 4:  $2\sigma$  and  $3\sigma$  contours obtained by fitting the shape of the SUSY signal di-jet mass spectrum for (a)  $m_{\tilde{q}} = 650$  GeV, and (b)  $m_{\tilde{q}} = 1$  TeV. As in Fig. 1, the shaded area on the upper-left is excluded because the slepton is either lighter than neutralino or below 100 GeV. The jaggedness of the contours is due to Monte Carlo statistics.

The  $m_{T2}$  variable is an extension of the well-known transverse mass ( $m_T$ ) [22] for the case of two invisible final state daughters. For the one step cascade decay considered here (see Eq. (1)), we have:

$$m_{T2}(m_x) = \min_{\mathbf{p}_T(D_1) + \mathbf{p}_T(D_2) = \mathbf{E}_T^{\text{miss}}} [\max(m_T^{(1)}, m_T^{(2)})]$$

with

$$m_T^{(i)} = \sqrt{m_x^2 + 2(E_T(q_i)E_T(D_i) - \mathbf{p}_T(q_i) \cdot \mathbf{p}_T(D_i))},$$

where  $D = \tilde{Z}_1$ ,  $P = \tilde{q}$ ,  $m_x$  is the trial daughter mass and the final state quark masses have been neglected. The minimization on the right-hand-side is carried out over the partitions of the  $\mathbf{E}_T^{\text{miss}}$  vector. Since  $m_{T2}(m_x = m_D) \leq m_P$ , the value of  $m_{T2}^{\text{max}}(m_D)$  determines the parent's mass. However, because the LSP mass ( $m_D$ ) is not known, in general it is not possible to obtain the parent mass  $m_P$  (the squark mass in our case). It can be shown that for *any* value of the trial LSP mass  $m_x$ ,

$$m_{T2}^{\text{max}}(m_x) = E_0 + \sqrt{E_0^2 + m_x^2}, \quad (6)$$

with  $E_0 = (m_{\tilde{q}}^2 - m_{\tilde{Z}_1}^2)/2m_{\tilde{q}}$ . Thus for any value of  $m_x$ , a determination of  $m_{T2}^{\text{max}}$  serves to determine<sup>6</sup>  $E_0$ . Assuming that  $m_{\tilde{Z}_1}^2/m_{\tilde{q}}^2 \ll 1$ , this reduces to a determination of the squark

<sup>6</sup>Of course, this simple analysis will be affected by the altered kinematics from gluino events contributing to the di-jet sample, and also by QCD radiative corrections.

mass. In this respect, the information that we get from an  $m_{T2}$  analysis is identical<sup>7</sup> to that we obtain using the method that we have described in Sec. 4.1. In our analysis we take  $m_x = 0$  to obtain,

$$m_{T2}^{max}(m_x = 0) = 2E_0 \approx m_{\tilde{q}}. \quad (7)$$

We show the  $m_{T2}(m_x = 0)$  distributions for the SUSY points  $(m_{\tilde{q}}, m_{\tilde{g}}) = (650, 667)$  GeV and  $(1000, 1030)$  GeV after the cuts of Eq. (2) in Fig. 5. We see that the distributions show distinct edges around 660 GeV and 1 TeV for the  $m_{\tilde{q}} = 650$  GeV and 1 TeV cases, respectively. To extract the  $m_{T2}^{max}$  value from the  $m_{T2}$  distributions we fit a “linear kink function” for a selected bin range on either side of the visible edge. The error for the fit includes the signal and BG statistical errors added in quadrature, as discussed in Sec.4.2. With this procedure, for the two case studies we obtain at  $2\sigma$ :

$$\begin{aligned} (m_{\tilde{q}}, m_{\tilde{g}}) = (650, 667) \text{ GeV} & : m_{\tilde{q}} = 640 - 682 \text{ GeV} \\ (m_{\tilde{q}}, m_{\tilde{g}}) = (1, 1.03) \text{ TeV} & : m_{\tilde{q}} = 970 - 1030 \text{ GeV} \end{aligned} \quad (8)$$

We see that for the lighter squark mass case for which we were able to use the dip structure, the error is essentially the same with both methods, whereas for the heavier squark case, the  $m_{T2}$  analysis yields a somewhat lower error<sup>8</sup>.

The squark mass result for the first SUSY point is shifted towards higher values than the true value. This is due to the  $\tilde{g}\tilde{g}$  contamination, which tends to mimic  $\tilde{q}\tilde{q}$  events with a heavier squark mass. On the other hand, the 1 TeV squark case has a much smaller contamination of  $\tilde{g}\tilde{g}$  events ( $< 10\%$ ) and  $m_{T2}^{max}$  in this case provides the correct value for  $m_{\tilde{q}}$ .

Before ending this section, we list the pros and cons of the extraction of the squark mass from  $m_{T2}$  or from the di-jet mass distribution described here.

- Clearly, the di-jet mass method is inapplicable if the squark is much heavier than the gluino, since then the di-jet signal from squark production is very small. In this regime,  $m_{T2}$  is clearly superior as it potentially offers the possibility of determining both  $m_{\tilde{g}}$  and  $m_{\tilde{Z}_1}$ .
- If  $m_{\tilde{q}} \simeq m_{\tilde{g}}$ , and the integrated luminosity of the LHC is large enough to enable us to utilize the dip structure in the  $m_{jj}$  mass distribution, the two procedures yield the same information (*i.e.* a measure of  $m_{\tilde{q}}$  if  $m_{\tilde{Z}_1}^2 \ll m_{\tilde{q}}^2$ ), and with comparable precision. The di-jet mass distribution also offers the possibility of constraining  $m_{\tilde{g}}$ . This can then be compared with a direct determination of  $m_{\tilde{g}}$  from the independent multi-jet event sample using, for instance,  $m_{\text{eff}}$ . Consistency of the gluino mass obtained from these *independent* data samples would bolster the case that the new physics is indeed supersymmetry.

---

<sup>7</sup>It has been suggested [23] that if the squark pair is produced with a high transverse momentum ( $\sim m_{\tilde{q}}$ ) it may be possible, in principle, to determine both  $m_{\tilde{q}}$  and  $m_{\tilde{Z}_1}$  separately using the  $m_{T2}$  procedure. We note, however, that under 1% of squark pairs will be produced with these large values of the pair transverse momentum, and so do not pursue this any further in our study.

<sup>8</sup>We have verified that both the central and error values for  $m_{\tilde{q}}$  is weakly dependent on the choice of the trial mass  $m_x$ . The magnitude of the error is, however, somewhat sensitive to the number of bins on both side of the kink that we use in our fit. We have shown a conservative range in Eq.(8) above.

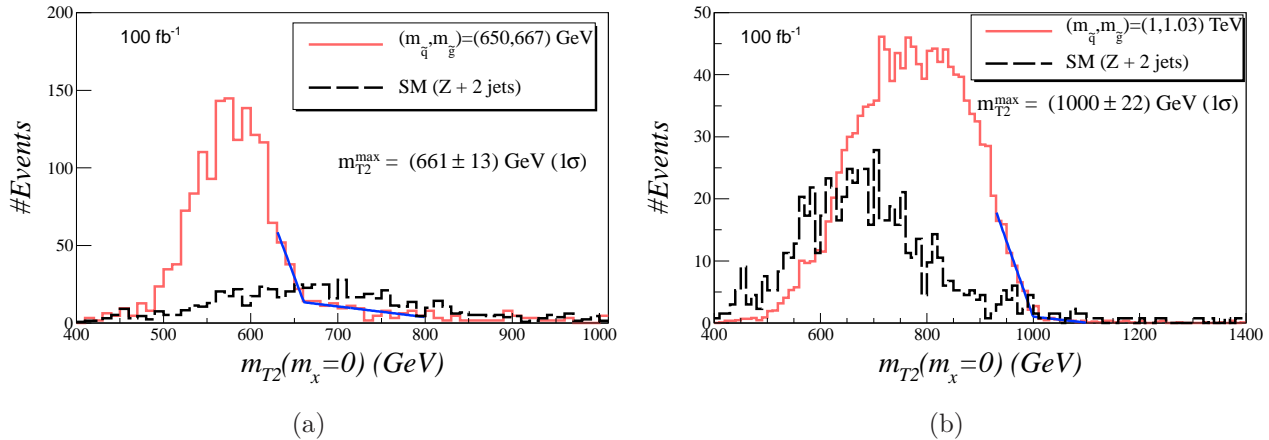


Figure 5: The  $m_{T2}$  distribution for (a)  $(m_{\tilde{q}}, m_{\tilde{g}}) = (650, 667)$  GeV and (b)  $(m_{\tilde{q}}, m_{\tilde{g}}) = (1000, 1030)$  GeV SUY points in Fig 4 after the cuts in Eq. (2) of the text. The trial LSP mass is set to zero. The straight lines show the “linear kink fit” to the signal, and is used to extract  $m_{T2}^{max}$ . The dashed histogram shows the  $m_{T2}$  distribution for the dominant SM BG (Z + 2 jets). We also show the  $m_{T2}^{max}$  value obtained from the fit and its  $1\sigma$  error.

- In our analysis, we have assumed that the squarks that lead to di-jet events (mostly  $\tilde{u}_R$  and  $\tilde{d}_R$  for mSUGRA) are essentially degenerate in mass. If these had a small but significant mass splitting, the shape of the  $m_{jj}$  distribution would likely be distorted and we would extract some sort of averaged mass. The  $m_{T2}$  analysis, on the other hand, relies on an end-point (which the mass splitting may smear) and would yield the larger of the squark masses.
- Our method for extracting  $m_{\tilde{q}}$  relies only on the jet energies and angles, whereas  $m_{T2}$  also requires  $E_T^{miss}$ . While the jet energy scale is likely to be the largest experimental systematic uncertainty for mass extraction from the  $m_{jj}$  distribution, the  $m_{T2}$  procedure relies on the entire detector, and so is likely to have different experimental systematics.

## 6 Summary

We have proposed a new way to determine the squark mass using templates to fit the *shape* of the invariant mass distribution of acollinear dijet events at the LHC. Standard model backgrounds are suppressed by cuts on  $\alpha$ ,  $\Delta\phi_{jj}$ ,  $E_T^{tot}$  and veto of isolated leptons. Our analysis is independent of many details of the underlying model, and requires only that at least some types of squarks have a large branching ratio for direct decays to the LSP. It yields a measure of the squark mass if  $m_{Z_1}^2 \ll m_{\tilde{q}}^2$ . While the signal may have sizable  $E_T^{miss}$ , imposing a  $E_T^{miss}$  cut does not lead to a qualitative improvement on the precision with which the squark mass is determined.

We emphasize that the squark mass is determined by a fit to only the shape of the signal di-jet invariant mass spectrum. If  $m_{\tilde{g}} \simeq m_{\tilde{q}}$ , the signal may also get a significant contribution

from  $\tilde{g}\tilde{q}$  production which, like squark pair production, is fixed by SUSY QCD<sup>9</sup> in terms of just  $m_{\tilde{q}}$  and  $m_{\tilde{g}}$ . We do not make use of the magnitude of the signal which would depend on model-dependent branching fractions for squark and gluino decay. Indeed, the gluino contamination and/or the dependence of the squark  $E_T$  spectrum on  $m_{\tilde{g}}$  also allows us to constrain  $m_{\tilde{g}}$ , albeit with considerably lower precision than  $m_{\tilde{q}}$ .

As discussed in Sec. 4.1 and in more detail in the Appendix, the cuts on  $\alpha$  and  $E_T^{tot}$  serve a dual role. Aside from background reduction, with appropriate choices  $\alpha > 0.5$  (the natural value to discriminate the signal from mismeasured QCD di-jet events) and  $E_T^{tot} \gtrsim m_{\tilde{q}}$  cuts, we have shown that signal events with intermediate values of  $m_{jj}$  pass the cuts with reduced efficiency compared to events with high and low di-jet masses. The resulting dip structure in the di-jet mass distribution (see the inset in Fig. 3a) is very sensitive to the value of  $m_{\tilde{q}}$ , and so increases the precision with which the squark mass can be extracted if the integrated luminosity is high enough to allow the implementation of a hard enough cut on  $E_T^{tot}$ .

We have performed two case studies, each with the gluino just slightly heavier than the squark, to investigate the precision with which it is possible to extract the squark mass from the dijet distribution. Our results are shown in Fig. 4. We see that for the  $m_{\tilde{q}} = 650$  GeV case for which the dip structure in the di-jet mass distribution should be visible in LHC experiments with an integrated luminosity of  $100 \text{ fb}^{-1}$ , the squark mass is constrained to lie between 630-690 GeV at  $2\sigma$ , while for a 1 TeV squark for which the  $100 \text{ fb}^{-1}$  is not sufficient to utilize the dip structure, the corresponding range is 935-1040 GeV. We find that in the former case the precision that we obtain is essentially the same as that we would obtain using  $m_{T2}$ , but the systematics of the two measurements are quite different.

The method that we have proposed using the analysis of di-jet events from supersymmetry to determine the squark mass can be generalized to other beyond the SM theories and used to determine the characteristic heavy particle mass. The invariant mass construction relies only on kinematical cuts, the assumption of a low mass of the stable (invisible) particle and a large enough branching ratio for the two body decay of the heavy particle into a jet and the invisible lighter particle.

## Acknowledgments

XT thanks the UW IceCube collaboration and the UW Phenomenology Institute for making his visit to the University of Wisconsin, where part of this work was carried out, possible. This research is supported in part by grants from the US Dept. of Energy and by the Fulbright Program and CAPES (Brazilian Federal Agency for Post-Graduate Education).

## Appendix: The Dijet Invariant Mass

The di-jet invariant mass in Fig. 3 shows distinct features after the cuts in Eq. (2). Here we present a discussion of the kinematics behind these distinct shapes and how they relate to

---

<sup>9</sup>To be technically precise, we do assume that intra-generational squark mixings are negligible.

the squark mass. For tractability, we neglect QCD radiation, SUSY contamination and SM backgrounds.

As we will see below, the dip structure in the  $m_{jj}$  distribution that we have discussed at length in the text mostly arises from the  $E_T^{tot} \equiv E_T(j_1) + E_T(j_2)$  and  $\alpha$  cuts, hence we shall omit the  $\Delta\phi_{jj}$  cut to start with. Since  $m_{jj}$ ,  $\alpha$  and  $E_T^{tot}$  are invariant under longitudinal boosts along the beam axis (the  $Z$ -direction) and rotations, we can restrict our analysis to the squark-pair center of mass frame, with the momentum of both squarks in the  $XZ$  plane:

$$\begin{aligned}\tilde{q}_1^\mu &= \gamma m_{\tilde{q}}(1, \beta \sin \theta, 0, \beta \cos \theta), \\ \tilde{q}_2^\mu &= \gamma m_{\tilde{q}}(1, -\beta \sin \theta, 0, -\beta \cos \theta),\end{aligned}\tag{9}$$

where  $\beta$  is the speed of the squarks, and  $\gamma = 1/\sqrt{1-\beta^2}$ . The jet energy in the squark rest frame is  $E_0 = (m_{\tilde{q}}^2 - m_{Z_1}^2)/2m_{\tilde{q}}$ . Its value in the squark-pair rest frame is changed by the boost, but is typically of this order. A hard jet (as required by  $E_T^{tot} \gtrsim 2E_0$ ) results when the daughter quark is roughly collinear with its parent squark. In order to satisfy the hard  $E_T^{tot}$  cut, we will for simplicity, make the approximation that the hardest quark is parallel to its parent squark, which fixes its four-momentum to be,

$$q_1^\mu = \gamma E_0(1 + \beta)(1, \sin \theta, 0, \cos \theta).\tag{10}$$

However,  $\theta_{\tilde{q}_2 q_2}$ , the angle between  $\tilde{q}_2$  and  $q_2$  in the squark center-of-mass frame is not necessarily restricted to small values and  $q_2$  can be emitted in any direction, although, before cuts,  $\theta_{\tilde{q}_2 q_2} = 0$  still is the most likely value if the squark is significantly boosted. The four-momentum of the second quark can be written as:

$$\begin{aligned}q_2^\mu &= E_0 [\gamma(1 + \beta \cos \theta_0), -\gamma \sin \theta (\cos \theta_0 + \beta) + \cos \theta \sin \theta_0 \cos \phi_0, \sin \theta_0 \sin \phi_0, \\ &\quad -\gamma \cos \theta (\cos \theta_0 + \beta) - \sin \theta \sin \theta_0 \cos \phi_0],\end{aligned}$$

where  $\pi - \theta_0$  and  $\phi_0$  are the polar and azimuthal angles of  $q_2$  in the  $\tilde{q}_2$  rest frame (with axes oriented so that  $\tilde{q}_2$  is moving along the negative  $Z$ -axis), respectively. The  $q_2$ - $\tilde{q}_2$  angle in the squark CM frame ( $\theta_{\tilde{q}_2 q_2}$ ) is then related to  $\cos \theta_0$  through:

$$\cos \theta_{\tilde{q}_2 q_2} = \frac{\beta + \cos \theta_0}{1 + \beta \cos \theta_0},$$

, while the dijet invariant mass ( $m_{jj}$ ) is given by

$$m_{jj} = \sqrt{2}\gamma E_0(1 + \beta)\sqrt{1 + \cos \theta_0}.\tag{11}$$

We now proceed to investigate the shape of the  $m_{jj}$  distribution under the constraints:

$$\alpha > 1/2 \text{ and } E_T^{tot} > 2E_0.\tag{12}$$

Toward this end, we consider three distinct cases:

- A)  $\cos \theta_{\tilde{q}_2 q_2} \approx 1 \Leftrightarrow \cos \theta_0 \approx 1$ , corresponding to high  $m_{jj}$  values,

- B)  $\cos \theta_{\bar{q}_2 q_2} = 0 \Leftrightarrow \cos \theta_0 = -\beta$ , corresponding to intermediate  $m_{jj}$  values, and
- C)  $\cos \theta_{\bar{q}_2 q_2} \approx -1 \Leftrightarrow \cos \theta_0 \approx -1$ , corresponding to low  $m_{jj}$  values.

*Case A).* This configuration corresponds to  $q_2$  emitted nearly along its parent direction. Completely back to back jets ( $\theta_0 = 0$ ) always have  $\alpha \leq 1/2$  and therefore can never satisfy Eq.(12). Thus, we take  $\theta_0 = 0 + \epsilon$ , where  $0 < \epsilon \ll 1$ . Then  $\alpha$  and  $E_T^{tot}$  become:

$$\alpha \approx \frac{\sin \theta}{2} - \epsilon \sqrt{\frac{1-\beta}{1+\beta}} \frac{\cos \theta \cos \phi_0}{2} \quad \text{and} \quad E_T^{tot} \approx 2E_0 \left[ \sqrt{\frac{1+\beta}{1-\beta}} \sin \theta - \epsilon \frac{\cos \theta \cos \phi_0}{2} \right] \quad (13)$$

We see from the expression for  $\alpha$  above that the constraint  $\alpha > 0.5$  eliminates events with back-to-back (or nearly back-to-back) jets, as does the  $\Delta\phi < 1.5$  cut in (2) of the text. This is, of course, why it so effectively reduces the QCD background [16]. The highest di-jet mass events after the cuts nevertheless arise from acollinear hard jets with large opening angle between them, though without the  $\alpha$  cut this distribution would extend out to even higher  $m_{jj}$  values.

*Case B).* This configuration corresponds to the case where  $q_2$  is emitted perpendicular to its parent direction and consequently also perpendicular to  $q_1$ . The expressions for  $\alpha$  and  $E_T^{tot}$  are:

$$\alpha = \sqrt{\frac{1-\beta}{2}} \sqrt{\cos^2 \theta \cos^2 \phi_0 + \sin^2 \phi_0} \quad \text{and} \quad E_T^{tot} = \sqrt{\frac{1+\beta}{1-\beta}} E_0 [\sin \theta + (1-\beta) \sqrt{\cos^2 \theta \cos^2 \phi_0 + \sin^2 \phi_0}] \quad (14)$$

If we impose  $\alpha > 1/2$ , we have:

$$\sqrt{\cos^2 \theta \cos^2 \phi_0 + \sin^2 \phi_0} > \frac{1}{\sqrt{2(1-\beta)}} \Rightarrow \beta < 1/2$$

For  $\phi_0 = \pi$  or 0 we have:

$$E_T^{tot} = \sqrt{\frac{1+\beta}{1-\beta}} E_0 [\sin \theta + (1-\beta) |\cos \theta|]$$

The above expression is maximum for  $\sin^2 \theta = 1/(2 - 2\beta + \beta^2)$ , which gives:

$$E_T^{tot} < \sqrt{\frac{1+\beta}{1-\beta}} E_0 \sqrt{1 + (1-\beta)^2} < \sqrt{\frac{15}{4}} E_0$$

for  $\beta < 1/2$ . Therefore, for  $\phi_0 = \pi$  or 0 (*i.e.* the quarks, the squarks and the proton beam are all in one plane), Eq. (12) can never be satisfied. On the other hand, if we look at extremely acoplanar configurations with  $\phi_0 = \pi/2$  or  $3\pi/2$ :

$$E_T^{tot} = \sqrt{\frac{1+\beta}{1-\beta}} E_0 [\sin \theta + (1-\beta)] \leq \sqrt{\frac{27}{4}} E_0 \approx 2.6 E_0$$



We see that such cases are allowed by our cuts. However, imposing  $E_T^{tot} > 2E_0$  requires large values of  $|\sin \phi_0|$  – we have verified numerically that, for Case B,  $E_T^{tot} > 2E_0$  requires  $|\sin \phi_0| \gtrsim 0.75$  – considerably restricting the phase space for configurations that simultaneously satisfy the  $\alpha$  and  $E_T^{tot}$  cuts. This analysis, therefore, confirms the qualitative reasoning in Sec. 4.1 of the text for the existence of the dip at intermediate  $m_{jj}$  values. More importantly this analysis quantifies the magnitude of the cut on  $E_T^{tot}$  that is needed for the appearance of the dip. Increasing the cut to  $E_T^{tot} \gtrsim 2.6E_0$  would completely suppress this configuration accentuating the dip even further, but this harder cut would lead to a considerable reduction in the statistics.

*Case C*). Finally, in this case,  $q_2$  is emitted anti-parallel to its parent and consequently parallel to  $q_1$ . This is, of course, an oversimplification, since the two would-be jets would then be merged into a single jet by our cone algorithm for defining jets, which is why we write the expression for  $\alpha$  allowing an angle  $\epsilon$  between  $q_2$  and its parent squark. Taking  $\theta_0 = \pi - \epsilon$ , with  $0 < \epsilon \ll 1$ , we find that,

$$\alpha \approx \frac{\sin \theta(1 - \beta)}{(1 + \beta)\epsilon} \quad \text{and} \quad E_T^{tot} \approx 2E_0\gamma \sin \theta, \quad (15)$$

independent of  $\phi_0$ . We readily see that this small  $m_{jj}$  momentum configuration can easily satisfy the cuts in Eq. (12). We point out that a *very large* squark boost would make this configuration less likely. It is thus possible that a very hard cut on  $E_T^{tot}$  would eliminate most events with very low values of  $m_{jj}$ , causing the dip structure to wash out altogether.

To see how the semi-quantitative analysis with the three cases that we have just discussed stands up to inclusion of *all* events from squark pair production we show in Fig. 6 a scatter plot of  $m_{jj}$  versus  $\cos \theta_{\tilde{q}_2 q_2}$  in the squark CM frame, after the  $\alpha > 1/2$  and  $E_T^{tot} > 800$  GeV cuts have been applied, but with  $\theta_{\tilde{q}_1 q_1}$  and  $\phi_0$  allowed to take all values. Events with an azimuthal angle separation  $\Delta\phi$  larger (smaller) than 1.5 are depicted by stars (dots). The points cluster at high  $m_{jj}$  values ( $\cos \theta_{\tilde{q}_2 q_2} \sim 1$ ), as expected, since the squark boost causes the  $\cos \theta_{\tilde{q}_2 q_2}$  distribution to peak at  $\theta_{\tilde{q}_2 q_2} = 0$ . We see that the bulk of these events have  $\Delta\phi > 1.5$ . On the other hand, for intermediate  $m_{jj}$  values ( $\cos \theta_{\tilde{q}_2 q_2} \approx 0$ ), which corresponds to Case B discussed above, relatively few events pass the cuts. Once we move to large negative values of  $\cos \theta_{\tilde{q}_2 q_2}$  (Case C), the kinematical configuration once again satisfies the cuts, even though the squark boost tends to suppress emission in this direction. We thus see how the double-peaked  $m_{jj}$  profile shown in Fig. 3a arises, once we require  $E_T^{tot} > 700$  GeV,  $\alpha > 0.5$  and  $\Delta\phi_{jj} < 1.5$  to increase the signal cross-section and reduce the SM background. As can be seen from Fig.6, the  $\Delta\phi_{jj} < 1.5$  cut suppresses the high  $m_{jj}$  values but does not change the double-peaked structure.

Finally, our analysis also makes clear that if we reduce the cut on  $E_T^{tot}$  and allow events with  $E_T^{tot} \lesssim 2E_0$ , kinematic configurations of Case B will be allowed for any  $\phi_0$  value and the cut suppression of intermediate  $m_{jj}$  values will no longer occur, causing the dip to disappear. We then expect the invariant mass distribution to present a single peak at intermediate  $m_{jj}$ . This is indeed what happens in Fig.3b for the  $(m_{\tilde{q}}, m_{\tilde{g}}) = (1000, 1030)$  GeV point, where  $E_0 = 490$  GeV and the cuts are  $E_T^{tot} > 700$  GeV,  $\alpha > 0.5$  and  $\Delta\phi_{jj} < 1.5$ .

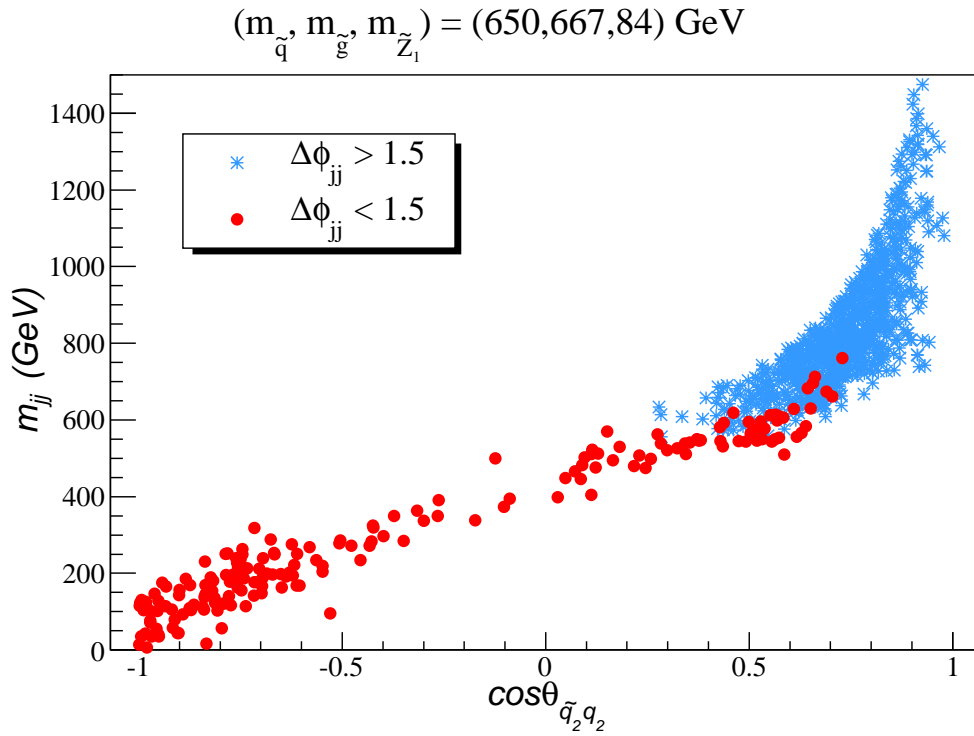


Figure 6: A scatter plot of the invariant dijet mass ( $m_{jj}$ ) versus the quark-squark angle  $\theta_{\tilde{q}_2 q_2}$  for  $(m_{\tilde{q}}, m_{\tilde{g}}, m_{\tilde{Z}_1}) = (650, 667, 84) \text{ GeV}$ , after the  $E_T^{tot} > 800 \text{ GeV}$  and  $\alpha > 0.5$  cuts have been applied. The (blue) star points have  $\Delta\phi_{jj} > 1.5$ , while the (red) dot points have  $\Delta\phi_{jj} < 1.5$

## References

- [1] For reviews of SUSY, see H. Baer and X. Tata, *Weak Scale Supersymmetry: From Superfields to Scattering Events*, (Cambridge University Press, 2006); M. Drees, R. Godbole and P. Roy, *Theory and Phenomenology of Sparticles*, (World Scientific, 2004); P. Binetruy, *Supersymmetry* (Oxford University Press, 2006); S. P. Martin, hep-ph/9709356.
- [2] H. Baer, C. H. Chen, F. Paige and X. Tata, *Phys. Rev. D* **52** (1995) 2746 and *Phys. Rev. D* **53** (1996) 6241; H. Baer, C. H. Chen, M. Drees, F. Paige and X. Tata, *Phys. Rev. D* **59** (1999) 055014 H. Baer, C. Balázs, A. Belyaev, T. Krupovnickas and X. Tata, *J. High Energy Phys.* **0306** (2003) 054; see also, S. Abdullin and F. Charles, *Nucl. Phys. B* **547** (1999) 60; S. Abdullin *et al.* (CMS Collaboration), *J. Phys. G* **28** (2002) 469; B. Allanach, J. Hetherington, A. Parker and B. Webber, *J. High Energy Phys.* **08** (2000) 017.
- [3] ATLAS Detector and Physics Performance: Technical Design Report, V. 2, CERN-LHCC-99-15.
- [4] CMS Collaboration, *J. Phys. G* **34** (2007) 995.
- [5] I. Hinchliffe *et al.* *Phys. Rev. D* **55** (1997) 5520 and *Phys. Rev. D* **60** (1999) 095002; H. Bachacou, I. Hinchliffe and F. Paige, *Phys. Rev. D* **62** (2000) 015009.
- [6] H. Baer, K. Hagiwara and X. Tata, *Phys. Rev. D* **35** (1987) 1598; H. Baer, D. Dzialo-Karatas and X. Tata, *Phys. Rev. D* **42** (1990) 2259; H. Baer, C. Kao and X. Tata, *Phys. Rev. D* **48** (1993) 5175; H. Baer, C. H. Chen, F. Paige and X. Tata, *Phys. Rev. D* **50** (1994) 4508.
- [7] H-C. Cheng *et al.*, *J. High Energy Phys.* **0712** (076) 2007 and *Phys. Rev. D* **80** (2009) 035020.
- [8] C. Lester and D. Summers, *Phys. Lett. B* **463** (1999) 99; A. Barr, C. Lester and D. Summers, *J. Phys. G* **29** (2003) 2343; W. S. Cho, K. Choi, Y. Kim and C. Park, *Phys. Rev. Lett.* **100** (2008) 171801 and *J. High Energy Phys.* **0802** (2008) 035; H-C. Cheng and Z. Han, *J. High Energy Phys.* **0812** (2008) 063.
- [9] C. Lester and a Barr, *J. High Energy Phys.* **0712** (2007) 102; B. Gripaios, *J. High Energy Phys.* **0802** (2008) 053; A. Barr, B. Gripaios and C. Lester, *J. High Energy Phys.* **0911** (2009) 096.
- [10] K. Matchev, F. Moortgat, L. Pape and M. Park, *J. High Energy Phys.* **0908** (2009) 104.
- [11] J. Alwall, A. Freitas and O. Mattelaer, *AIP Conf.Proc.* **1200** (2010) 442.
- [12] T. Han, I. Kim and J. Song, *Phys. Lett. B* **693**, 575 (2010), arXiv:0906.5009.
- [13] H. Baer, V. Barger, G. Shaughnessy, H. Summy and L. t. Wang, *Phys. Rev. D* **75**, 095010 (2007); V. Barger, G. Shaughnessy and B. Yenko, *Phys. Rev. D* **83**, 055006 (2011).
- [14] W. S. Cho *et al.*, Ref.[8]
- [15] M. Burns, K. Kong and K. Matchev, *J. High Energy Phys.* **0903** (2009) 143.
- [16] L. Randall and D. Tucker-Smith, *Phys. Rev. Lett.* **101** (2008) 221803.
- [17] H. Baer, V. Barger, A. Lessa and X. Tata, *J. High Energy Phys.* **0909** (2009) 063.

- [18] M. Genest, arXiv:0912.4378 [hep-ex]; N. Ozturk, arXiv:0910.2964 [hep-ex].
- [19] ISAJET, by H. Baer, F. Paige, S. Protopopescu and X. Tata, hep-ph/0312045; see also H. Baer, J. Ferrandis, S. Kraml and W. Porod, *Phys. Rev. D* **73** (2006) 015010.
- [20] V. Khachatryan *et al.*, *Phys. Lett. B* **698** (2011) 196; The ATLAS Collaboration, *Phys. Rev. Lett.* **106** (2011) 131802. For earlier limits from Tevatron experiments see, T. Aaltonen *et al.* *Phys. Rev. Lett.* **102** (2009) 121801; V. Abazov *et al.* *Phys. Lett. B* **660** (2008) 449.
- [21] M. L. Mangano, M. Moretti, F. Piccinini, R. Pittau and A. D. Polosa, *JHEP* **0307**, 001 (2003)
- [22] V. Barger and R.J.N. Phillips, *Collider Physics*, (Addison-Wesley, 1987)
- [23] A.J. Barr, B. Gripaios and C.G. Lester, *JHEP* **0802**, 014 (2008)